

Age dependent modes of extensional necking instability in soft glassy materials

D. M. Hoyle and S. M. Fielding

*Department of Physics, Durham University, Science Laboratories,
South Road, Durham DH1 3LE, United Kingdom*

(Dated: July 15, 2018)

We study the instability to necking of an initially cylindrical filament of soft glassy material subject to extensional stretching. By numerical simulation of the soft glassy rheology model and a simplified fluidity model, and by analytical predictions within a highly generic toy description, we show that the mode of instability is set by the age of the sample relative to the inverse of the applied extensional strain rate. Young samples neck gradually via a liquid-like mode, the onset of which is determined by both the elastic loading and plastic relaxation terms in the stress constitutive equation. Older samples fail at smaller draw ratios via a more rapid mode, the onset of which is determined only by the solid-like elastic loading terms (though plastic effects arise later, once appreciable necking develops). We show this solid-like mode to be the counterpart, for elastoplastic materials, of the Considère mode of necking in strain-rate-independent solids.

PACS numbers: 83.60.Wc, 83.10.-y, 83.50.Jf, 83.80.-k

Many soft materials, including foams, emulsions, microgels and colloids comprise disordering packings of mesoscopic substructures: foam bubbles, emulsion droplets, *etc.* At high volume fractions, the local rearrangement dynamics of these are impeded by large energy barriers and show a glassy slowing down. This underpins many universal features in the rheological (deformation and flow) properties of these “soft glassy materials” (SGMs). Particularly striking is the phenomenon of rheological ageing, in which an initially liquid-like sample slowly evolves towards an ever more solid-like state as a function of the time since it was prepared. In the last decade, significant progress has been made in understanding the role of ageing in the shear flow of SGMs [1]. Similar phenomena have been explored in polymeric [2] and metallic [3] glasses, with many unifying features across all these amorphous, elastoplastic materials.

Much less is understood about the response of these materials to extensional deformations, which are important to industrial processes in fibre spinning, ink-jetting, porous media, and the peeling and tack of surfaces bonded by adhesives. In the standard experimental test, an initially near uniform cylindrical (or rectangular) sample is steadily drawn out in length, with the aim of measuring the tensile stress as a function of strain and strain rate. Ubiquitously observed, however, is an instability to neck formation: the sample thins more quickly in the middle than at its endpoints (Fig. 1) and eventually fails. This has been observed in emulsions [4–8], laponite suspensions, [8–10], foams [11–13], polymer glasses [14, 15], simulations of shear transformation zone models [16, 17], and in shear thickening colloids [18–21] (though our focus here is on shear thinning SGMs).

A hallmark of all these elastoplastic materials is that their deformation properties depend strongly on the *rate* at which strain is applied, particularly when ageing is present. For *rate-independent* materials, the onset of necking was predicted by Considère in 1885 [22] to coin-

cide with a regime of declining tensile force as a function of strain. But despite the accumulating body of observations described above, counterpart criteria for necking in elastoplastic materials remain lacking (though for an insightful early study of rate dependence, see [23]). The contribution of this Letter is to provide such criteria, in the form of general analytical results supported by numerical simulation of two widely used models of soft glasses. In this way, we argue these new criteria to apply universally across all ageing elastoplastic materials and so to have the same, highly general status as the Considère criterion for rate-independent solids.

Importantly, we find the mode of instability to necking to be determined by the age t_w of the sample, relative to the inverse of the applied extensional (Hencky) strain rate $\bar{\epsilon}$: young samples ($\bar{\epsilon}t_w \ll 1$) fail by a gradual, liquid-like mode, whereas old samples ($\bar{\epsilon}t_w \gg 1$) show a fast, solid-like failure mode. We further show this solid-like mode to be the counterpart for elastoplastic materials of the Considère mode in rate-independent solids. In this way, crucially, the physics of a material’s failure is predicted to be governed by a switch between two qualitatively distinct modes of instability, governed simply by

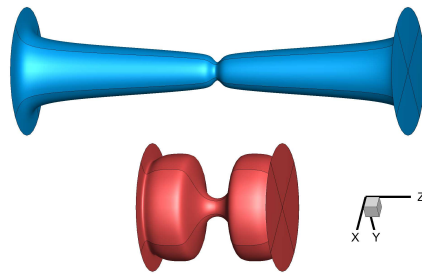


FIG. 1. Necked profiles. Extension rate shown by arrow in Fig. 2. Top: young sample, $t_w = 10^2$. Bottom: old, $t_w = 10^4$.

the sample age [24].

We consider incompressible, inertialess deformations for which the velocity and stress fields in the material, $\mathbf{v}(\mathbf{r}, t)$ and $\mathbf{T}(\mathbf{r}, t)$, obey standard conditions of mass balance, $\nabla \cdot \mathbf{v} = 0$, and force balance, $\nabla \cdot \mathbf{T} = 0$. The total stress $\mathbf{T} = \boldsymbol{\Sigma} + 2\eta\mathbf{D} - p\mathbf{I}$ comprises an elastoplastic contribution $\boldsymbol{\Sigma}$ from the mesoscopic substructures, a Newtonian solvent contribution of viscosity η , and an isotropic pressure. Here $K_{\alpha\beta} = \partial_\beta v_\alpha$ and $\mathbf{D} = \frac{1}{2}(\mathbf{K} + \mathbf{K}^T)$.

For the dynamics of the elastoplastic stress $\boldsymbol{\Sigma}$ we adopt the soft glassy rheology (SGR) model [25]. This considers an ensemble of elements, each corresponding to a local mesoscopic region of material. Under an imposed deformation, each element experiences a buildup of local elastic stress, intermittently released by plastic relaxation events. The treatment of tensorial stresses [26] within SGR was inspired by the Doi-Ohta model of dense emulsions [27], and considers a local density function $f(\mathbf{n})$ for the area (per unit volume) of droplet interfaces normal to \mathbf{n} , with a spherical normalisation $Q = \int d\mathbf{n}f(\mathbf{n})$ and stress $\boldsymbol{\Sigma} = G \int d\mathbf{n}(\mathbf{nn} - \frac{1}{3}\mathbf{I})f(\mathbf{n})$. The constant modulus $G = 1$ sets our stress scale. The buildup of elastic stress in any element during deformation obeys [27]

$$\begin{aligned} (\partial_t + \mathbf{v} \cdot \nabla)\boldsymbol{\Sigma} &= \boldsymbol{\Sigma} \cdot \mathbf{K} + \mathbf{K}^T \cdot \boldsymbol{\Sigma} + \frac{2}{3}Q\mathbf{D} - \boldsymbol{\Sigma} : \mathbf{K} \left(\frac{2}{3}\mathbf{I} + \frac{\boldsymbol{\Sigma}}{Q} \right), \\ (\partial_t + \mathbf{v} \cdot \nabla)Q &= \mathbf{K} : \boldsymbol{\Sigma}. \end{aligned} \quad (1)$$

Relaxation of stress by local plastic yielding events is modelled as hopping of the elements over strain-modulated energy barriers, governed by a noise temperature x . Upon yielding, any element resets its local stress to zero and selects its new energy barrier at random from an exponential distribution. This distribution confers a broad spectrum of yielding times $P(\tau)$, resulting in a glass phase with a yield stress for $x < 1$. Full details of the model in its original, spatially uniform form are in Ref. [25, 26], and in its adaptation to spatially non-uniform shear flows in Ref. [28]. The counterpart adaptation for non-uniform extension is summarised in [29].

Because the SGR model is numerically rather cumbersome, we shall also present results for a simplified fluidity model in which SGR's full spectrum of yield times $P(\tau)$ is replaced by a single characteristic relaxation timescale τ . The RHS of Eqs. 1 then acquire relaxation terms: $-\frac{1}{\tau}Q\boldsymbol{\Sigma}$ and $-\frac{1}{\tau}\mu Q^2$ for the $\boldsymbol{\Sigma}$ and Q dynamics respectively. Here μ is a phenomenological parameter with $0 \leq \mu \leq 1$ [27]. A standard ‘‘fluidity’’ model for the dynamics of τ ,

$$(\partial_t + \mathbf{v} \cdot \nabla)\tau = 1 - \sqrt{2\mathbf{D} : \mathbf{D}}(\tau - \tau_0), \quad (2)$$

then captures the two essential ingredients of the SGR model: (i) ageing without flow, in which the relaxation time increases with the time since sample preparation, $\tau \sim t$; and (ii) rejuvenation by flow, which restores a steady state with $\tau = \tau_0 + 1/\sqrt{2\text{Tr}\mathbf{D} : \mathbf{D}}$. We choose units in which the microscopic time $\tau_0 = 1$.

We consider an initially cylindrical sample of length L_0 and radius R_0 , freshly prepared at time $t = 0$ in a fluidized state with $\tau = \tau_0$ and $\boldsymbol{\Sigma} = \mathbf{0}$. It is then left to age undisturbed during a time $t_w \gg \tau_0$, before being steadily drawn out such that for times $t > t_w$ the length increases as $\dot{L} = \bar{\epsilon}(t)L$, with the cross sectional area correspondingly thinning. We present results below for two common protocols: (a) constant rate of Hencky strain $\bar{\epsilon}$, corresponding to $L = L_0 \exp[\bar{\epsilon}(t - t_w)]$, and (b) constant rate \dot{L} of length increase, corresponding to a progressively declining strain rate $\bar{\epsilon} = (1/\bar{\epsilon}_0 + t - t_w)^{-1}$.

For convenience, we solve the models within an one-dimensional (1D) approximation [29–31], in which the wavelengths of any variations that develop along the filament are assumed long compared to the radius. This standard assumption [32–34] has been shown to perform surprisingly well even some way into the regime where the wavelengths become comparable to the radius. It allows the neglect of any radial dependencies, such that the deformation of a filament extended in the z direction is characterised simply by its cross-sectional area $A(z, t)$ and an area averaged z -component of velocity $v(z, t)$.

A choice must then be made for how to model the no-slip condition where the sample ends meet the experimental endplates. A good approximation [35–37] for initial aspect ratios $\Lambda = L_0/R_0 \geq 1$ is to invoke a divergent viscosity over a small region of the filament near each plate, acting to pin the fluid to the plates. (Equivalently, this region can be thought of as *part* of the plates.) We adopt this assumption [29], and have checked that the physics reported is robust to it by also performing simulations (not shown) with periodic boundary conditions (corresponding to a stretched torus, without endplates).

We neglect surface tension, restricting to the development of a neck in a highly elastoplastic filament in which bulk stresses dominate. Clearly, surface tension must ultimately become important in the very final stages of breakup, once the radius becomes small [38]. However our focus is not on the details of that final pinch-off, but on the time at which necking first becomes appreciable, which we define as the centrepoint-radius having fallen to 15% of the initial radius.

The basic phenomenon that we seek to explain is shown in Fig. 1. This displays the necked profiles of two filaments: one that has been drawn relatively slowly compared to the inverse age and another that has been drawn more quickly. As can be seen, the slowly drawn filament survives to a relatively longer draw ratio before approaching failure, and displays a gradual necking profile. In contrast, the rapidly drawn filament fails sooner and with a more pronounced, cusp-like profile.

That basic observation is quantified for the fluidity model in Fig. 2, for protocol (a) in which the Hencky strain rate $\bar{\epsilon}$ is held constant and the sample ends separate exponentially. The symbols show the draw ratio $L(t)/L_0$ at which appreciable necking becomes appar-

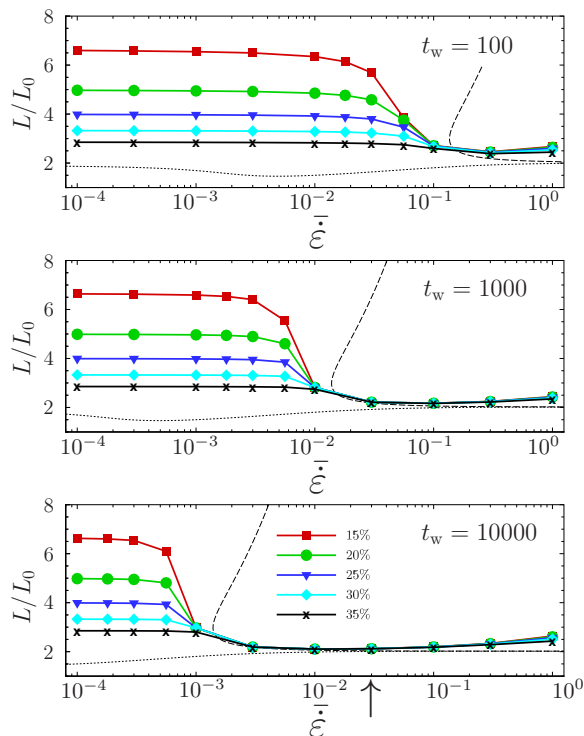


FIG. 2. Fluidity model in protocol a). Solid lines: draw ratio at which the radius of the filament at its thinnest point has fallen to 35%, 30% \dots 15% of the initial filament radius (curves upwards). Data are shown for three different initial sample ages (panels downwards). Initial aspect ratio $\Lambda = 2$. Dotted lines: Considère criterion [22]. Dashed lines: counterpart of the Considère criterion for elastoplastic materials. Parameters: $\mu = 0.1$ and $\eta = 0.01$. Arrow shows $\bar{\epsilon}$ for Fig. 1.

ent, versus that applied strain rate. As can be seen, old samples ($\bar{\epsilon}t_w \gg 1$) fail at a modest draw ratio L/L_0 , while young samples ($\bar{\epsilon}t_w \ll 1$) survive to a larger L/L_0 . Also shown (dotted line) is the Considère criterion at which the tensile force first starts declining with strain. This would signal necking onset in a rate-independent solid but evidently performs badly here for young samples $\bar{\epsilon}t_w < O(1)$. We return below to discuss this in the context of an alternative criterion shown by the dashed lines. Fig. 3 confirms the same behaviour in the SGR model. The same behaviour is also seen [29] in protocol (b), which has a constant drawing rate $\dot{L} = \bar{\epsilon}_0 L_0$ and progressively decreasing strain rate $\bar{\epsilon} = (1/\bar{\epsilon}_0 + t - t_w)^{-1}$.

To allow analytical insight, let us consider now a highly simplified, toy description of an elastoplastic filament in extensional deformation. The relevant dynamical quantities are the area profile $A(z, t)$, the z -component of velocity $v(z, t)$, the strain rate field $\dot{\epsilon}(z, t) = \partial_z v(z, t)$, with the overall applied strain rate $\bar{\epsilon}(t) = \int_0^L dz \dot{\epsilon}(z, t)/L$, the elastoplastic stress $GZ(z, t)$, which we write as a constant modulus G times a strain-like variable Z , the total tensile stress $\sigma_E(z, t) = GZ + 3\eta\dot{\epsilon}$, and force $F(t) = \sigma_E A$.

These obey the conditions of mass and force balance:

$$\begin{aligned} \partial_t A + v \partial_z A &= -\dot{\epsilon} A \\ 0 &= \partial_z (A \sigma_E). \end{aligned} \quad (3)$$

We then choose for Z the simplest possible dynamics that combines elastic loading (f) and plastic relaxation (g):

$$\partial_t Z + v \partial_z Z = \dot{\epsilon} f(Z) - \frac{1}{\tau} g(Z). \quad (4)$$

We intentionally leave the forms of f and g unspecified, in order to derive below general instability criteria that do not depend on particular choices. For simplicity we do not include in this toy description explicit dynamics for τ , but below comment on predictions when $\bar{\epsilon}\tau \gg 1$ and $\bar{\epsilon}\tau \ll 1$, thereby inserting ageing $\tau \sim t_w$ “by hand”.

Within this toy model, we consider an initially near uniform cylindrical filament and express its state as the sum of a time-dependent uniform base state, corresponding to a perfect cylinder being stretched, plus small amplitude heterogeneous perturbations. Accordingly we write $a(u, t) = \bar{a} + \delta a_q \exp(iqu)$, $Z = \bar{Z}(t) + \delta Z_q \exp(iqu)$, $\dot{\epsilon}(u, t) = \bar{\epsilon}(t) + \delta \dot{\epsilon}_q \exp(iqu)$, choosing for convenience to work in the coextending, cothinning frame by defining transformed length and area variables $u = z \exp(-\bar{\epsilon})$ and $a = A \exp(\bar{\epsilon})$. We then perform a linear stability analysis to determine the time at which these heterogeneous perturbations start to grow, corresponding to the onset of necking. Substituting into Eqns. 3 and expanding in powers of the perturbation amplitude gives at first order

$$\partial_t \begin{pmatrix} \delta a \\ \delta Z \end{pmatrix}_q = \mathbf{M}_q(t) \cdot \begin{pmatrix} \delta a \\ \delta Z \end{pmatrix}_q, \quad (5)$$

in which the stability matrix \mathbf{M} has inherited the time-dependence of the uniform base state.

At least one eigenvalue of \mathbf{M} being positive at any time t then gives a strong indication that the heterogeneous perturbations will be growing at that time, corresponding to the development of necking. (Direct integration of the linearised equations confirms this, and also agrees with the early-time growth of a neck in a full nonlinear solution.) In fact it is straightforward to show that \mathbf{M}_q has two distinct modes of instability. One of these, which we call mode 1, has an eigenvalue of order $\bar{\epsilon}$ that is positive when the tensile stress of the underlying base state obeys $\bar{\epsilon}f' - \frac{1}{\tau}g' = \sigma_E'/\sigma_E < 0$. It is liquid-like in the sense that its onset is determined by an interplay between elastic loading (specified by f) and plastic relaxation (via g). The other (mode 2) has a much larger eigenvalue of order G/η that is positive when the base state $\sigma_E - Gf > 0$: its onset condition is set only by the solid-like elastic loading term f , independent of g [39].

These analytics explain our numerical results in the SGR and fluidity models as follows. We indeed see a mode directly analogous to mode 1, the onset of which involves both the elastic loading and plastic relaxation dynamics, and which involves significant plastic relaxation

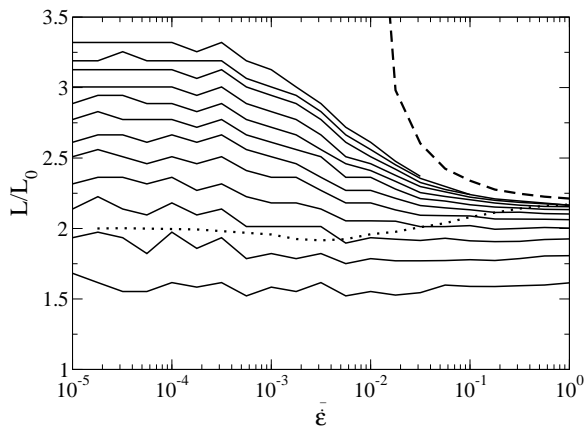


FIG. 3. SGR model in protocol a). Solid contour lines upward show where initial area perturbations have increased in amplitude by successive powers of 1.4. The initial area profile was seeded such that $A = 1 + \xi \cos(2\pi u)$, where $\xi = 3 \cdot 10^{-4}$. Dotted line: Considère criterion. Dashed line: counterpart criterion for elastoplastic material. Parameters: $x = 0.3$, $\lambda = 1.5$, $t_w = 10^2$.

along the entire filament. Its quantitative onset criterion is however modified compared with the toy model, due to the higher dynamical dimensionality of the full models: it is actually unstable for all strain rates and at all times during stretching. Any small perturbations to an initially cylindrical profile therefore start slowly growing as soon as stretching starts, for all strain rates. It is this mode that eventually leads to failure at relatively large L/L_0 for young samples $\bar{\epsilon}t_w \ll 1$ in Figs. 2 and 3.

For old samples, the solid-like mode 2 intervenes to cause failure at smaller strains. Its onset criterion $\sigma_E - Gf > 0$ transcribes (once cast into the forms of (7,8) below) unmodified to the fluidity and SGR models (and indeed any model, however complex). It is shown by the dashed line in Figs. 2 and 3, and is only satisfied if $\bar{\epsilon}\tau \gg 1$, *i.e.* in old samples for which $\bar{\epsilon}t_w \gg 1$. It is furthermore only met a finite time after the start of stretching. Once unstable, however, its much larger eigenvalue $O(G/\eta)$ gives much more rapid necking and the sample fails very shortly after instability onset, at only modest draw ratios. (This mode would in principle restabilise at higher strains, as seen in Fig. 2 by the doubling-back of the dashed line, but that is irrelevant because the filament will have failed by then.)

How do we understand this instability criterion, $\sigma_E - Gf > 0$ of mode 2? Noting that the tensile force $F = A\sigma_E$, we have (for the underlying base state)

$$\frac{\partial F}{\partial \epsilon} = A \left(-\sigma_E + \frac{\partial \sigma_E}{\partial \epsilon} \right) = A \left(-\sigma_E + Gf - G \frac{g}{\epsilon \tau} \right). \quad (6)$$

This follows from Eqns. 3 and 4, neglecting terms $O(\eta/G)$. Were the Considère criterion to apply directly, that would give instability for $\sigma_E - Gf + Gg/\epsilon\tau > 0$. However the dotted lines in Figs. 2 and 3 show this cri-

terion to perform poorly for young samples $\bar{\epsilon}t_w < O(1)$. We can, though, define a modified derivative,

$$\frac{\partial F}{\partial \epsilon} \Big|_{\text{elastic}} = A (-\sigma_E + Gf), \quad (7)$$

in which the plastic relaxation term is artificially switched off over the strain increment in question. We thereby recognise the onset of mode 2 instability as

$$\frac{\partial F}{\partial \epsilon} \Big|_{\text{elastic}} < 0. \quad (8)$$

It is this criterion that is marked as a dashed line in Figs. 2 and 3. It performs much better for these ageing materials, over the full range of $\bar{\epsilon}t_w$, than the original Considère criterion. It coincides with Considère only for $\bar{\epsilon}t_w \gg 1$: in this regime, the material behaves essentially as a nonlinear elastic solid (with $\epsilon f \gg \frac{g}{\tau}$), at least until necking first arises. (Once appreciable necking occurs it causes plastic flow in the thinning, central region of the filament.) Accordingly, we propose (8) as the counterpart for rate-dependent elastoplastic materials of the Considère criterion for rate-independent solids.

Finally, we have checked that our results are robust to reasonable variations in the values of the initial aspect ratio Λ and the Newtonian viscosity η ; and that they apply robustly over large regions of the space of the phenomenological parameters μ (fluidity) and λ, x (SGR, within its glass phase $x < 1$). See the SI for details [29].

To summarise, we have shown the instability to necking of a filament of soft glassy material to proceed by one of two possible modes. Young samples neck gradually via a mode informed by both elastic loading and plastic relaxation. Old samples fail more suddenly via a mode in which onset is informed only by elastic loading, and which is the counterpart for elastoplastic materials of the Considère mode of rate-independent solids. A particularly appealing feature of the physical picture presented here is this crossover between two distinct modes of instability, determined simply by the age of the sample relative to the inverse stretching rate. Having shown this numerically in two widely used models of soft glasses, as well as analytically, we argue these predictions to apply generically to all ageing elastoplastic materials. Indeed they may apply even more generally still, to pasty materials with long relaxation timescales τ but much weaker ageing effects, now set by the value of the inverse strain rate relative to τ . It remains an open challenge to understand how, within SGR, these ductile failure modes cross over to brittle cracking at even higher strain rates, for samples with notch-like initial imperfections [40, 41].

Acknowledgements — The research leading to these results has received funding from the European Research Council under the European Union's Seventh Framework Programme (FP7/2007-2013) / ERC grant agreement number 279365.

-
- [1] S. M. Fielding, P. Sollich, and M. E. Cates, *J. Rheology* **44**, 323 (2000).
- [2] L. C. E. Struik, *Physical aging in amorphous polymers and other materials* (Elsevier, Houston, 1978).
- [3] H. S. Chen, *Reports On Progress In Phys.* **43**, 353 (1980).
- [4] F. M. Huisman, S. R. Friedman, and P. Taborek, *Soft Matter* **8**, 6767 (2012).
- [5] N. Niedzwiedz, H. Buggisch, and N. Willenbacher, *Rheologica Acta* **49**, 1103 (2010).
- [6] S. R. Derkach, *Advances in Colloid and Interface Science* **151**, 1 (2009).
- [7] E. Miller, C. Clasen, and J. P. Rothstein, *Rheologica Acta* **48**, 625 (2009).
- [8] P. Coussot and F. Gaulard, *Physical Review E* **72**, 031409 (2005).
- [9] A. Shaukat, A. Sharma, and Y. Joshi, *Rheologica Acta* **49**, 1093 (2010).
- [10] A. Shaukat, M. Kaushal, A. Sharma, and Y. M. Joshi, *Soft Matter* **8**, 10107 (2012).
- [11] M. Arciniaga, C.-C. Kuo, and M. Dennin, *Colloids and Surfaces A: Physicochemical and Engineering Aspects* **382**, 36 (2011).
- [12] C.-C. Kuo and M. Dennin, *Journal of Rheology* **56**, 527 (2012).
- [13] C.-C. Kou and M. Dennin, *Physical Review E* **87**, 030201 (2013).
- [14] H. -N. Lee, K. Paeng, S. F. Swallen, and M. D. Ediger, *Science* **323**, 231 (2009).
- [15] J. Rottler, *Journal of Physics: Condensed Matter* **21** (2009).
- [16] L. O. Eastgate, J. S. Langer, and L. Pechenik, *Physical Review Letters* **90**, 045506 (2003).
- [17] C. H. Rycroft and F. Gibou, *Journal of Computational Physics* **231**, 2155 (2012).
- [18] P. J. Zimoch, G. H. McKinley, and A. E. Hosoi, *Physical Review Letters* **111**, 036001 (2013).
- [19] M. Roché, H. Kellay, and H. A. Stone, *Physical Review Letters* **107**, 134503 (2011).
- [20] M. I. Smith, R. Besseling, M. E. Cates, and V. Bertola, *Nature communications* **1** (2010).
- [21] M. Chellamuthu, E. M. Arndt, and J. P. Rothstein, *Soft Matter* **5**, 2117 (2009).
- [22] M. Considère, *Ann Ponts Chaussees* **9**, 574 (1885).
- [23] J. W. Hutchinson and K. W. Neale, *Acta Metallurgica* **25**, 839 (1977).
- [24] Note however related work on dependence on age (via initial condition) of crack propagation from a notch [41].
- [25] P. Sollich, F. Lequeux, P. Hebraud, and M. E. Cates, *Phys. Rev. Lett.* **78**, 2020 (1997).
- [26] M. E. Cates and P. Sollich, *J. Rheology* **48**, 193 (2004).
- [27] M. Doi and T. Ohta, *Journal of Chemical Physics* **95**, 1242 (1991).
- [28] S. M. Fielding, M. E. Cates, and P. Sollich, *Soft Matter* **5**, 2378 (2009).
- [29] See Supplemental Material at [*c.f. below*] for a description of the one dimensional approximation, transformation to coextending and cothinning reference frame, no-slip boundary condition and results for the constant velocity protocol. We also discuss the robustness to variations in the parameter choices made in the main text.
- [30] M. M. Denn, C. J. S. Petrie, and P. Avenas, *AIChE Journal* **21**, 791 (1975).
- [31] D. O. Olagunju, *Journal of Non-Newtonian Fluid Mechanics* **87**, 27 (1999).
- [32] M. Yao and G. H. McKinley, *Journal of Non-Newtonian Fluid Mechanics* **74**, 47 (1998).
- [33] M. Tembely, D. C. Vadiillo, M. R. Mackley, and A. Soucemarianadin, *Journal of Rheology* **46**, 159 (2012).
- [34] D. C. Vadiillo, M. Tembely, N. F. Morrison, O. G. Harlen, M. R. Mackley, and A. Soucemarianadin, *Journal of Rheology* **56**, 1491 (2012).
- [35] Y. M. Stokes, E. O. Tuck, and L. W. Schwartz, *Q. J. Mech. appl. Math.* **53**, 565 (2000).
- [36] C. Clasen, J. Eggers, M. A. Fontelos, J. Li, and G. H. McKinley, *Journal of Fluid Mechanics* **556**, 283 (2006).
- [37] P. Szabo, G. H. McKinley, and C. Clasen, *Journal of Non-Newtonian Fluid Mechanics* **169–170**, 26 (2012).
- [38] The contributions to force balance of the viscoelastic stresses and surface tension are respectively $G\partial_z\Sigma$ and (at leading order) $\gamma\partial_zR^{-1}$ where gamma is the coefficient of surface tension and R the radius of the filament.
- [39] Constitutive models that are too oversimplified to address the physics soft glasses, such as the Oldroyd B model, have an elastic loading term of trivially simple form and this mode 2 instability criterion is never met.
- [40] M. L. Falk, *Phys. Rev. B* **60**, 7062 (1999).
- [41] C. H. Rycroft and E. Bouchbinder, *Physical Review Letters* **109**, 5 (2012).

Supplemental Material for:
Age dependent modes of extensional necking instability in soft glassy materials

Coordinate transformation

FLUIDITY MODEL

In this section, we detail a one-dimensional approximation [S1, S2] in which the wavelengths of any variations along the filament are assumed long compared to the filament's radius. We also describe a transformation to the frame of reference that coextends and cothins with the overall average deformation of the filament. We then discuss the implementation of the no-slip condition where the filament meets the experimental endplates.

One dimensional approximation

We adopt a one dimensional approximation [S1, S2] that allows us to neglect any dependencies in the radial direction and consider only those in the coordinate z along the length of the filament. The cross sectional area is denoted $A(z, t)$ and the area-averaged local z -component of velocity is denoted $v(z, t)$. The local elongation rate at any point along the filament is $\dot{\epsilon} = \partial_z v$.

The continuity equation then reads

$$\partial_t A + v \partial_z A = -A \dot{\epsilon}. \quad (\text{S1})$$

The force balance condition imposes that the tensile force in the filament is independent of z ,

$$\partial_z F = 0. \quad (\text{S2})$$

The force F is the product of the area of the filament multiplied by the tensile stress:

$$F(t) = A(\Sigma + 3\eta\dot{\epsilon}), \quad (\text{S3})$$

where the tensile stress comprises additive viscoelastic and Newtonian contributions. Here the scalar viscoelastic stress difference $\Sigma = \Sigma_{zz} - \Sigma_{xx}$, where x denotes a radial coordinate. We then write $\Sigma = G\tilde{\Sigma}$ where the constant modulus $G = 1$ in our units, defining a strain like variable $\tilde{\Sigma}$, then drop the tilde for clarity.

The constitutive equations for the viscoelastic stress then read

$$\partial_t \Sigma + v \partial_z \Sigma = \dot{\epsilon} \left(Q - \frac{\Sigma^2}{Q} - \Sigma \right) - \frac{1}{\tau} Q \Sigma, \quad (\text{S4})$$

$$\partial_t Q + v \partial_z Q = \dot{\epsilon} \Sigma - \frac{1}{\tau} \mu Q^2. \quad (\text{S5})$$

The equation of motion for the relaxation time τ finally becomes

$$\partial_t \tau + v \partial_z \tau = 1 - (\tau - \tau_0) \sqrt{3} |\dot{\epsilon}|. \quad (\text{S6})$$

In this section, we describe an affine coordinate transformation to the co-extending and co-thinning frame. This removes the increase in sample length, which in the laboratory frame occurs as an exponential function of the spatially averaged Hencky strain $\bar{\epsilon}(t)$ applied to the filament. It also removes the corresponding exponential decrease in the filament's area. It renders numerical solution of the model much more straightforward, by removing the need for an adaptive mesh to address the changing sample length in the laboratory frame.

Accordingly, old variables $z, v, \dot{\epsilon}, A, F$ are transformed into new variables $u, w, \dot{\zeta}, a, f$ following:

$$z = u \exp[\bar{\epsilon}(t)], \quad (\text{S7})$$

$$v = [\dot{\bar{\epsilon}}(t)u + w(u, t)] \exp[\bar{\epsilon}(t)], \quad (\text{S8})$$

$$\dot{\epsilon} = \dot{\bar{\epsilon}}(t) + \dot{\zeta}(u, t), \quad (\text{S9})$$

$$A = A(0)a(u, t) \exp[-\bar{\epsilon}(t)], \quad (\text{S10})$$

$$F = A(0)f. \quad (\text{S11})$$

The other variables, Σ, Q and τ , are not transformed, but are now expressed as functions of the transformed space variable u and time t . The transformed equations of motion are then

$$f = \exp[-\bar{\epsilon}(t)] a [\Sigma + 3\eta(\dot{\bar{\epsilon}} + \dot{\zeta})], \quad (\text{S12})$$

$$\partial_t a + w \partial_u a = -\dot{\zeta} a, \quad (\text{S13})$$

$$\partial_t \Sigma + w \partial_u \Sigma = (\dot{\bar{\epsilon}} + \dot{\zeta}) \left(Q - \frac{\Sigma^2}{Q} - \Sigma \right) - \frac{1}{\tau} Q \Sigma \quad (\text{S14})$$

$$\partial_t Q + w \partial_u Q = (\dot{\bar{\epsilon}} + \dot{\zeta}) \Sigma - \frac{1}{\tau} \mu Q^2, \quad (\text{S15})$$

$$\partial_t \tau + w \partial_u \tau = 1 - (\tau - \tau_0) \sqrt{3} |\dot{\bar{\epsilon}} + \dot{\zeta}|. \quad (\text{S16})$$

To solve these equations numerically, a, Σ, Q and τ are updated at each time step using Eqns. S13 to S16. The updated values are then substituted into Eqn. S12. An appropriate integral of Eqn. S12 along the entire filament determines f , which is finally substituted back into Eqn. S12 to determine the strain rate profile $\dot{\bar{\epsilon}} + \dot{\zeta}(u, t)$ as a function of distance along the filament.

We choose our unit of length such that the initial length of the sample is unity. The sample domain is then $0 < u < 1$ for all times. The initial cross sectional area $A(0)$ defines the undeformed starting shape of the sample, with $a(u, 0) = 1$ for all u .

Endplates

The no-slip boundary condition where the ends of the sample meet the experimental endplates is imposed following Refs. [S3–S5], by invoking a divergent viscosity in a small layer of fluid near each end plate, acting to pin the fluid to the plates. (Equivalently, this region of very

high viscosity can effectively be thought of as forming *part* of the plates.) The viscosity takes the form

$$\eta(u) = \eta \left[1 + \frac{1}{32} \left(\frac{r_0 e^{-\bar{\epsilon}}}{u} \right)^2 + \frac{1}{32} \left(\frac{r_0 e^{-\bar{\epsilon}}}{1-u} \right)^2 \right], \quad (\text{S17})$$

in which r_0 is the initial radius of the filament.

SGR MODEL

Full details of the SGR model in its original, spatially uniform (zero-dimensional) form can be found in Refs. [S6, S7]. For a one-dimensional adaptation to spatially non-uniform shear flows, see Ref. [S8]. Here we detail the counterpart adaptation to non-uniform extensional flows in a filament of soft glass.

We divide the filament equally along its length into M sub elements, called bins for convenient shorthand in what follows. Each bin is initialised with the same area A_m and the same length L_m , corresponding to a uniform filament initially.

In each bin we place N SGR elements. Each element is initialised with a yield energy E_{mn} drawn randomly from the SGR model's prior distribution of trap depths $\rho(E) = \frac{1}{x_g} \exp(-E/x_g)$, where x_g is the glass transition temperature. In our numerics we use units in which $x_g = 1$. Each element is also assigned zero initial strain $\epsilon_{mn} = 0$ and correspondingly zero stress $\sigma_{mn} = 0$. The tensile viscoelastic stress in any bin is given as $\Sigma_m = \frac{1}{N} \sum_n \sigma_{mn}$ ($= 0$ initially).

We then evolve the dynamics at any timestep $t \rightarrow t + Dt$ by performing updates in three substeps, as follows.

In step 1, the elastic loading dynamics updates the strain of each SGR element according to $\epsilon_{mn} \rightarrow \epsilon_{mn} + \dot{\epsilon}_m Dt$, where $\dot{\epsilon}_m$ is the local strain rate in that element's bin. (This $\dot{\epsilon}_m = \bar{\epsilon}$ for the first timestep. In all subsequent timesteps it is updated in step 3 below.) Following Ref. [S7], the updated stress of each SGR element is prescribed from its updated strain as $\sigma_{mn} = 3GQ(\epsilon_{mn})$, in which

$$Q(\epsilon) = \frac{5}{8} \frac{1}{e^{3\epsilon} - 1} \left[e^{2\epsilon} - 2e^{-\epsilon} + (e^{5\epsilon} - 4e^{2\epsilon}) T(e^{3\epsilon} - 1) \right], \quad (\text{S18})$$

with the function

$$T(a) = \frac{\arctan(\sqrt{a})}{\sqrt{a}}. \quad (\text{S19})$$

(Note that this function Q (Eqn. S18) is distinct from the one used above for the fluidity model (Eqn. (1) in the main text). We use this notation Q here for consistency with that of Ref. [S7].) The strain of each bin is likewise updated as $\epsilon_m \rightarrow \epsilon_m + \dot{\epsilon}_m Dt$, the area as $A_m \rightarrow A_m \exp(-\dot{\epsilon}_m Dt)$ and the length as $L_m \rightarrow L_m \exp(\dot{\epsilon}_m Dt)$. The updated stress in each bin $\Sigma_m = \frac{1}{N} \sigma_{mn}$.

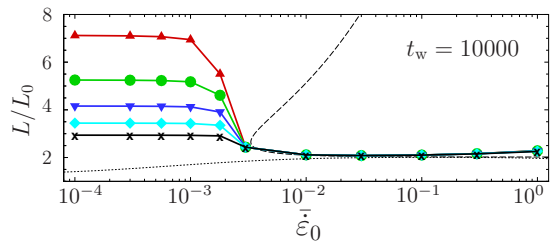


FIG. S1. Counterpart of Fig. 2 in the main text, for the fluidity model subjected to a constant velocity protocol (b), with a strain rate $(1/\bar{\epsilon}_0 + t - t_w)^{-1}$ that progressively decreases in time from an initial value $\bar{\epsilon}_0$. Solid lines: draw ratio at which the radius of the filament at its thinnest point has fallen to 35%, 30% \dots 15% of the initial filament radius (curves upwards). Initial aspect ratio, $\Lambda = 2$. Dotted lines: Considère criterion. Dashed lines: counterpart of the Considère criterion for elastoplastic materials. Parameters: $\mu = 0.1$ and $\eta = 0.01$.

In step 2, plastic relaxation is implemented by dynamics in which the probability of any SGR element hopping during any short time interval Dt is given by $r_{mn} Dt$. Following [S7], we take

$$r_{mn} = \frac{1}{\tau_0} \exp \left[-\frac{E_{mn} - \lambda R(\epsilon_{mn})}{x} \right] \quad (\text{S20})$$

which defines the parameter λ . The function R is given by,

$$R(\epsilon) = \frac{1}{2} \left[e^{-\epsilon} + e^{2\epsilon} T(e^{3\epsilon} - 1) \right] - 1. \quad (\text{S21})$$

Once a hop has occurred for any element n in bin m , its strain and stress are reset as $\epsilon_{mn} \rightarrow 0$, $\sigma_{mn} \rightarrow 0$, and its new yield energy is selected at random from the prior distribution $\rho(E)$.

Finally in step 3, force balance along the filament is implemented by realising that the force is the product of the area times the tensile stress, and that this must be uniform along the filament:

$$F_m = A_m [\Sigma_m + 3\eta \dot{\epsilon}_m] = F(t). \quad (\text{S22})$$

This allows us to calculate the force $F(t)$ as

$$F(t) \frac{1}{M} \sum_m \frac{1}{A_m} = \frac{1}{M} \sum_m Q(\Sigma_m) + 3\eta \bar{\epsilon}(t), \quad (\text{S23})$$

given a globally imposed average strain rate $\bar{\epsilon}(t)$ along the filament. This $F(t)$ is then finally fed back into Eqn. S22 in order to calculate the strain rate profile $\dot{\epsilon}_m$ along the filament.

As for the fluidity model, we choose units in which the modulus $G = 1$ and the microscopic time $\tau_0 = 1$. We also set the glass transition temperature $x_g = 1$.

CONSTANT DRAWING RATE (PROTOCOL B)

The results presented in the main text were for protocol (a) in which a constant rate of Hencky strain $\bar{\epsilon}$ is applied to the sample, corresponding to exponentially separating sample ends $L = L_0 \exp[\bar{\epsilon}(t - t_w)]$. As shown for the fluidity model in Fig. S1, the same behaviour is seen for protocol (b), which has a constant rate \dot{L} of length increase, corresponding to a progressively declining strain rate $\bar{\epsilon} = (1/\bar{\epsilon}_0 + t - t_w)^{-1}$.

ROBUSTNESS TO VARIATIONS IN PARAMETER VALUES

We have checked that our results are robust to reasonable variations in the initial aspect ratio $\Lambda = 1, 2, 3$, and in the value of the Newtonian viscosity η . Larger η cause the slight upturn of L/L_0 versus $\bar{\epsilon}$ for old samples $\bar{\epsilon}t_w > 1$ in Figs. 2 and 3 of the main text to be more pronounced: within this old-sample regime, more quickly drawn samples survive to higher L/L_0 . Our results also apply robustly over large regions of the space of the phenomenological parameters μ (fluidity) and λ, x (SGR, within its glass phase $x < 1$). For ‘less glassy’ samples (larger λ and larger x values approaching on-

set of the liquid phase at $x = 1$), more complicated effects are possible. However the basic phenomenon that we have reported remains robust even here: of relatively early failure onset determined by elastic loading alone for old samples $\bar{\epsilon}t_w \gg 1$, and failure onset delayed to larger L/L_0 also involving plastic relaxation for young samples $\bar{\epsilon}t_w \ll 1$.

-
- [S1] M. M. Denn, C. J. S. Petrie, and P. Avenas, *AIChE Journal* **21**, 791 (1975).
 - [S2] D. O. Olagunju, *Journal of Non-Newtonian Fluid Mechanics* **87**, 27 (1999).
 - [S3] Y. M. Stokes, E. O. Tuck, and L. W. Schwartz, *Q. J. Mech. appl. Math.* **53**, 565 (2000).
 - [S4] C. Clasen, J. Eggers, M. A. Fontelos, J. Li, and G. H. McKinley, *Journal of Fluid Mechanics* **556**, 283 (2006).
 - [S5] P. Szabo, G. H. McKinley, and C. Clasen, *Journal of Non-Newtonian Fluid Mechanics* **169–170**, 26 (2012).
 - [S6] P. Sollich, F. Lequeux, P. Hebraud, and M. E. Cates, *Phys. Rev. Lett.* **78**, 2020 (1997).
 - [S7] M. E. Cates and P. Sollich, *J. Rheology* **48**, 193 (2004).
 - [S8] S. M. Fielding, M. E. Cates, and P. Sollich, *Soft Matter* **5**, 2378 (2009).